Electrical contact properties between carbon nanotube ends and a conductive atomic force microscope tip

Masafumi Inaba, Kazuyoshi Ohara, Megumi Shibuya, Takumi Ochiai, Daisuke Yokoyama, Wataru Norimatsu, Michiko Kusunoki, and Hiroshi Kawarada

Citation: Journal of Applied Physics **123**, 244502 (2018); doi: 10.1063/1.5027849
View online: https://doi.org/10.1063/1.5027849
View Table of Contents: http://aip.scitation.org/toc/jap/123/24
Published by the American Institute of Physics

Electrical contact properties between carbon nanotube ends and a conductive atomic force microscope tip

Masafumi Inaba,[1,2] Kazuyoshi Ohara,[1] Megumi Shibuya,[1] Takumi Ochiai,[1] Daisuke Yokoyama,[1] Wataru Norimatsu,[2] Michiko Kusunoki,[2] and Hiroshi Kawarada[1,2,3,a)]
[1]*Graduate School of Advanced Science and Engineering, Waseda University, 3-4-1 Okubo, Shinjuku, Tokyo 169-8555, Japan*
[2]*Institute of Materials and Systems for Sustainability, Nagoya University, Furo-cho, Chikusa, Nagoya 464-8603, Japan*
[3]*The Kagami Memorial Laboratory for Materials Science and Technology, Waseda University, 2-8-26 Nishiwaseda, Shinjuku, Tokyo 169-0051, Japan*

(Received 6 March 2018; accepted 23 May 2018; published online 27 June 2018)

Understanding the electrical contact properties of carbon nanotube (CNT) ends is important to use the high conductance of CNTs in the CNT on-axis direction in applications such as through-silicon via structures. In this study, we experimentally evaluated the contact resistivity between single-/multi-walled CNT ends and a metal nanoprobe using conductive atomic force microscopy (C-AFM). To validate the measured end contact resistivity, we compared our experimentally determined value with that obtained from numerical calculations and reported values for side contact resistivity. The contact resistivity normalized by the length of the CNT ends was 0.6–2.4 $\times 10^6$ Ω nm for single-walled CNTs. This range is 1–2 orders of magnitude higher than that determined theoretically. The contact resistivity of a single-walled CNT end with metal normalized by the contact area was 2–3 orders of magnitude lower than that reported for the resistivity of a CNT sidewall/metal contact. For multi-walled CNTs, the measured contact resistivity was one order of magnitude higher than that of a CNT forest grown by remote plasma-enhanced chemical vapor deposition, whereas the contact resistivity of a top metal electrode was similar to that obtained for a single-walled CNT forest. *Published by AIP Publishing*. https://doi.org/10.1063/1.5027849

INTRODUCTION

Carbon nanotubes (CNTs) possess high electrical conductivity[1] and high current durability.[2] These excellent properties are advantageous for the use of CNTs for high current density conduction in a small area, such as metallization in highly miniaturized silicon (Si) ultra-large-scale integrated circuits (ULSI).[3–7] CNTs and their bundles are candidates to replace metal vertical interconnects (VIs) because CNTs do not suffer from electromigration and exhibit higher conductivity than Cu. To use the metallic properties of a CNT bundle/forest in metallization, particularly as a nanosized VI structure in a Si ULSI, it is important to enhance the density of CNT walls. Densely grown CNTs have been produced for large-scale integrated through-silicon via applications.[8–16] However, the CNT sidewall/metal contact of CNTs with caps on their ends is resistive.[17] To enhance their contact properties, CNTs with open end structures have been realized by chemical mechanical polishing (CMP),[18,19] but the resulting CNT end/metal contacts show wide variation in their behavior.[18] Thus, controlling the electrical contact properties of CNT ends is essential to use CNTs in electron/electrical devices with high current conductivity.

A CNT has two types of edges: the sidewall and the ends. Lateral-type devices such as thin-film transistors and sensing devices include CNTs with sidewall contacts, whereas vertical-type devices such as VIs contain CNTs with end contacts. CNT/CNT sidewall contacts[20–22] have been reported to exhibit tunneling conduction, and CNT sidewall/metal contact resistivity has been observed experimentally.[23] Electrical contact between a metal and CNT end has advantages over CNT sidewall/metal contact according to numerical studies.[24,25] These studies revealed that the contact resistivity depends on the length of graphene sheet edges, corresponding to CNT ends. Because of the difficulty of evaluating CNT end contact properties, the experimentally measured contact resistivity between a CNT end and metal has not yet been reported.

Conductive atomic force microscopy (C-AFM) has been used to measure the electronic transport properties of the edges of multi-walled CNTs[17,26] and single-walled CNTs because of the nanoscale contact of the sharp electrical probe. Because the C-AFM probe is coated with a low-resistivity metal, it is feasible to estimate the contact properties between an object and the coated metal. The contact resistance of multi-walled CNTs[27,28] and carbon nanofibers[29,30] grown independently has already been measured by C-AFM. However, quantitative contact resistivity, which is normalized by CNT wall length or CNT contact area, has not yet been evaluated for small-diameter CNTs, particularly densely packed single-walled CNT bundles. In the case of a densely packed CNT forest, the C-AFM probe can contact the CNT ends directly. Here, we measure the electrical contact between small-diameter single-walled CNT ends and a metal by C-AFM. We also examine the differences between the contact properties of single- and multi-walled CNTs.

a)E-mail: kawarada@waseda.jp

EXPERIMENTAL SECTION

To assess CNT/metal probe contacts, we used packed CNT forests formed by surface decomposition of silicon carbide (SiC) (referred to as CNT forests on SiC)[31] and dense CNT forests formed by remote plasma-enhanced chemical vapor deposition[32] (RPECVD), which are denoted as RPECVD CNT forests. Figures 1(a)–1(c) show schematic images of the current mapping setup for a CNT forest on SiC, RPECVD CNT forest, and CNT VI structure, respectively, formed by the processes described below. The electrical properties of CNT VI structures fabricated by a similar method to that in our previous report[18] were investigated using C-AFM (Nano-R, Pacific Nanotechnology, Inc., CA, USA).

The CNT forests on SiC were synthesized by the SiC surface decomposition method on conductive 4H-SiC substrates ($\sim 4 \times 10^{-2}$ Ω cm) by annealing at 1600 °C under vacuum ($\sim 10^{-2}$ Pa) to ensure the electrical contact between the CNTs and C-AFM nanoprobe. The resulting CNT forests were closely packed with a surface density of $\sim 3 \times 10^{12}$ cm^{-2}. Figure 1(d) shows a cross-sectional scanning electron microscopy (SEM) image of a CNT forest on SiC. The CNTs had a length of 200 nm. The back electrode was fabricated by sputtering Au and Ti layers on a Si substrate and then attaching the CNT forest on SiC to the back electrode using conductive paste. The current passed through the conductive SiC substrate.[33]

The RPECVD CNT forests were fabricated as follows. A 10-nm-thick Ti buffer layer and 500-nm-thick Au layer as a bottom electrode were deposited on a Si wafer by sputtering. A catalyst sandwich-like structure consisting of [Al (1 nm; top)/Fe (0.5 nm)/Al (5 nm; bottom)], in which Fe acted as a catalyst, was then deposited on the bottom electrode.[34] A CNT forest with a length of ~10 μm was synthesized by RPECVD at 600 °C. This CNT forest mainly consisted of single-walled CNTs with a diameter of 2–3 nm and high surface density of $\sim 10^{11}$ cm^{-2}.[35] Because the RPECVD CNTs were fabricated by bottom growth,[36] the CNTs were connected to the Fe catalyst particles on the bottom electrode. The CNTs were fixed to the substrate using spin-on-glass (SOG). Finally, the CNT caps at the top of CNT forest were removed by CMP[18] to give CNTs of various lengths (0.5–4.0 μm). Figure 1(e) shows a cross-sectional SEM image of a RPECVD CNT forest with a CNT length of 4 μm after CMP.

The VI structures filled with CNTs were fabricated by a similar method to that in Ref. 18. Briefly, a tetraethylorthosilicate dielectric layer was deposited on a Si substrate and then thin holes were formed in the dielectric layer by lithography with buffered hydrofluoric wet etching. The hole diameter was varied from 60 to 300 nm. To grow CNTs in the VI structures, Co catalyst particles were deposited on the Cu/Ta bottom electrode. CNTs were then synthesized by RPECVD at a low temperature of 390 °C. The average CNT diameter, wall number, and surface density were 7 nm, seven, and 1.6×10^{11} cm^{-2}, respectively. The CNTs were fixed using SOG, polished, and then their ends were removed by CMP. The CNT length was 270 nm. Figure 1(f) shows a cross-sectional transmission electron microscopy (TEM) image of a fabricated VI structure with a 100-nm diameter.

RESULTS AND DISCUSSION

It is important to determine if the C-AFM nanoprobe only contacts the CNT ends, but this is hard to confirm directly. We first evaluated the contact resistance between single-walled CNT ends and the C-AFM nanoprobe. To evaluate contact "resistivity," the contact area and number of contacting CNTs should be determined. Contact area was evaluated from the CNT on-axis resistance and current profile of the VI structure. To validate the evaluated end contact resistivity, we compared the obtained value to those estimated from a numerical study and reported for sidewall contact resistivity.

To confirm the CNT/probe contact, current maps of densely packed CNT forests on SiC were observed. Figures 2(a) and 2(b) show examples of a current map and current

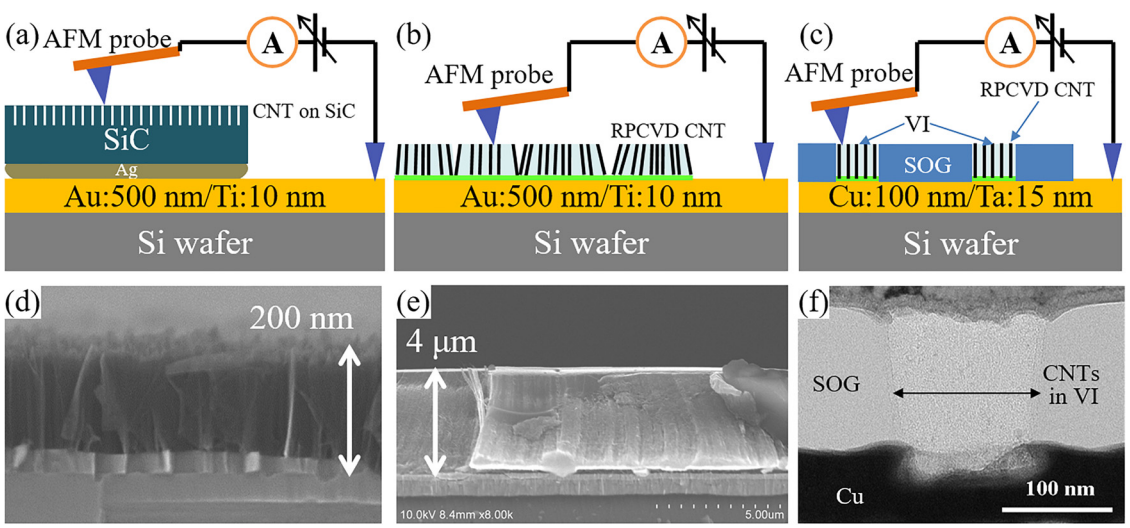

FIG. 1. Schematics of current mapping setups for (a) a carbon nanotube (CNT) forest on SiC, (b) remote plasma-enhanced chemical vapor deposition (RPECVD) CNT forest, and (c) vertical interconnect (VI) structure, respectively. Cross-sectional SEM images of (d) a CNT forest on SiC and (e) RPECVD CNT forest after chemical mechanical polishing, and (f) cross-sectional TEM image of a 100-nm-diameter VI structure filled with CNTs. SOG is spin-on-glass.

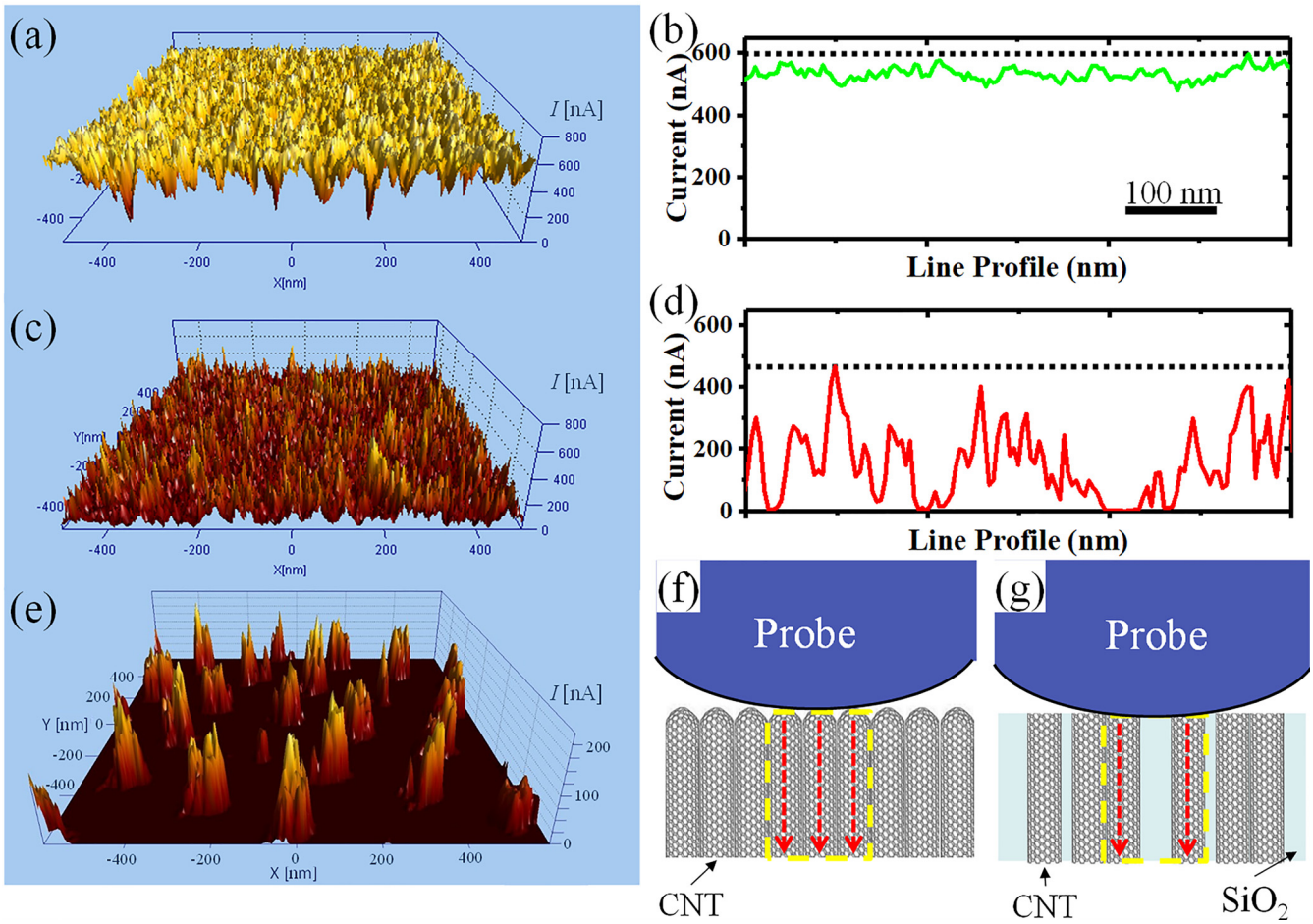

FIG. 2. Representative (a), (c), and (e) current maps and (b) and (d) current line profiles for (a) and (b) a CNT forest on SiC, (c) and (d) RPECVD CNT forest, and (e) aligned 80-nm-diameter VI structures filled with CNTs. CNT/AFM nanoprobe contact models for (f) a CNT forest on SiC, where the nanoprobe properly contacts the CNTs, and (g) a RPECVD CNT forest, where the nanoprobe incompletely contacts the CNTs.

line profile of a CNT forest with a CNT length of 100 nm on SiC, respectively. The vertical axis corresponds to the current obtained by applying a voltage. An almost homogeneous high-current region was observed with a few low-current spots. CNT ends contacted well with the C-AFM probe. We mainly used C-AFM nanoprobes made from $PtIr_5$ (PPP-EFM, Nanosensors^{TM}) in this study. Note that the current was almost the same when using Au nanoprobes (PPP-FMAu, Nanosensors^{TM}). This is because the contact is formed between the metal and metallic graphene sheets of the CNT ends.

The CNT forest formed by RPECVD has spaces between the CNT bundles. Figures 2(c) and 2(d) show a current map and current line profile of a RPECVD CNT forest, respectively. In contrast to the current map of the CNT forest on SiC, that of the RPECVD CNT forest is not homogeneous and has high-current peaks starting from zero current. The difference between the current maps of the CNT forest on SiC and RPECVD CNT forest originates from the surface density of the CNT bundles. The high-current regions of the CNT forest on SiC indicate effective contact between the conductive nanoprobe and densely packed CNT forest, as shown in Fig. 2(f). The AFM nanoprobe current for the CNT forest on SiC is uniform over the entire substrate. In contrast, there are random current peaks and valleys for the RPECVD CNTs with an average diameter of 2–3 nm and surface density of $\sim 10^{11}$ cm^{-2},[35] indicating that they are bundled locally rather than uniformly packed. Thus, the current peaks in Figs. 2(c) and 2(d) correspond to the electric current of locally packed CNT bundles. At the current peaks, the nanoprobe contacts some CNTs, as shown in Fig. 2(g), indicating that CNTs form packed bundles or loosely packed bundles with voids at the CNT bundle top. The peak with the highest current can be considered to represent the most conductive CNT bundle or strongest contact between the bundle and AFM nanoprobe. Figure 2(e) shows a current map of VI structures filled with CNTs. The current is observed only at the VI structures, indicating that the CNTs passed the current to the bottom electrode. The currents of the VI structures vary, but almost all VIs are conductive. Compared with the current maps of the RPECVD CNT forest, the current of the VI structures is smaller at a similar applied voltage.

Current–voltage curves for the CNT bundles were obtained from the relationship between the peak current of each current map and applied voltage. Figure 3(a) shows representative current–voltage curves for the RPECVD CNT forest. These curves were always straight at low voltages of up to 16 mV, indicating that the contact was ohmic. The resistance was obtained by dividing the applied voltage by the current.

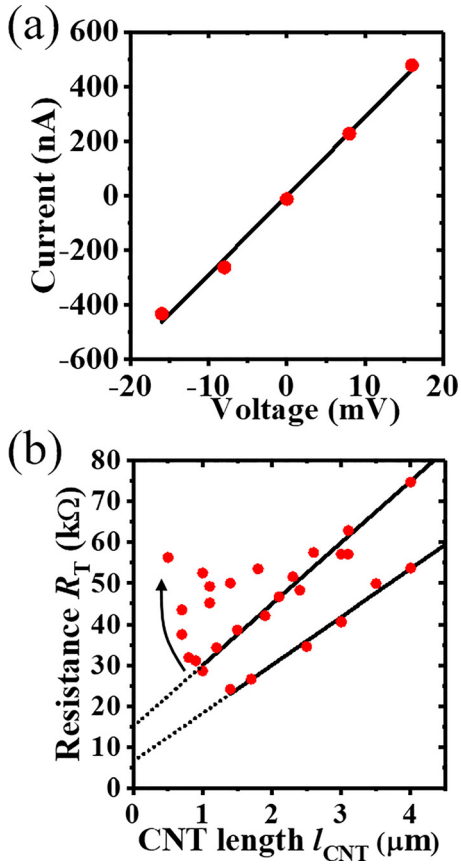

FIG. 3. (a) Representative current–voltage characteristics of a RPECVD CNT forest. The AFM nanoprobe/CNT contact was ohmic. (b) Relationship between measured resistance and CNT length for RPECVD CNT forests. Most of the data points fell on the two black lines. There was a tendency for the resistance to increase as the CNT length shortened below 1 μm (indicated by an arrow), which may indicate that CNTs do not form large bundles when they are shorter than 1 μm but do form bundles as the CNT length increases.

To further understand the determined resistance, we modeled the contact for the RPECVD CNT forest. Assuming that some CNTs contact the nanoprobe, the total resistance R_T corresponds to the sum of the individual CNT body resistance, individual CNT/nanoprobe contact resistance $R_{C,CNT/probe}$, and individual CNT/metal catalyst contact resistance $R_{C,CNT/cat}$ divided by the number of CNTs contacting the nanoprobe $n_{contact}$, that is,

$$R_T = \frac{R_{C,CNT/probe} + \rho_{CNT} l_{CNT} + R_{C,CNT/cat}}{n_{contact}}, \quad (1)$$

where ρ_{CNT} and l_{CNT} correspond to the resistivity of an individual CNT in the on-axis direction and its length, respectively. Here, we neglected the effects from neighboring CNTs on the contact area, which covered the area of the bottom contact, because the conductivity of the CNT forest in the in-plane direction was two orders of magnitude lower than that in the on-axis direction.[22,35] Note that the same method is not applicable to the CNT forest on SiC. This is because the resistivity of SiC is higher than that of the CNT on-axis, so the resistance of CNTs should be too low to determine the CNT bulk resistance.

To further investigate the electrical contact properties of the structures, we used the transfer length method. Figure 3(b) shows the relationship between the lowest measured resistance in each current map and CNT length for the RPECVD CNT forests. Here, the CNT forest height was measured from large-area topographic images. Because the PRCVD CVD forests were not densely packed, they formed a tabletop and valley structure after spin coating of SOG, as shown in Fig. S2 (supplementary material). The valleys reached the substrate. We considered that the CNT length was the measured height of the tabletops. The resistances of the RPECVD CNT forests were in the range of 25–75 kΩ and had a positive correlation with CNT length. Most of the data points fell on the two black lines in Fig. 3(b). A possible explanation for this result is the wear of the C-AFM nanoprobe.[37] Because the C-AFM nanoprobe scans the CNT forest structure many times, the contact area of the nanoprobe should gradually increase with the scan length. Although this behavior should be investigated further, we considered that the contact area was almost constant in the following discussion. The slope in Fig. 3(b) corresponds to $\rho_{CNT}/n_{contact}$. The slope of the black lines was 12–15 kΩ/μm. The reported on-axis ρ_{CNT} for an individual CNT in a RPECVD CNT forest is ~200 kΩ/μm,[35] so the calculated number of CNTs contacting the nanoprobe $n_{contact}$ is 13–17. Note that there was a tendency for the resistance to increase as the CNT length shortened below 1 μm, as indicated by the arrow in Fig. 3(b). This may indicate that CNTs shorter than 1 μm do not form bundles, whereas longer CNTs do form bundles. This behavior can be explained by the CNT growth mechanism.[38] CNTs grow randomly in the initial growth period and their ends become entangled. The CNTs then start to form forest-like structure as their length increases. CNTs should form bundles through the van der Waals attractive force in the bulk region but remain mechanically separated at their bottom ends, where they are connected to the underlying catalyst particles. Therefore, we neglected the data for the CNTs shorter than 1 μm.

Next, the contact resistivity was evaluated. By setting l_{CNT} to zero in Eq. (1), the total of the top-end and bottom-end contact resistances of the CNTs is expressed as

$$R_T|_{l_{CNT}=0} \equiv \frac{R_{C,total}}{n_{contact}} = \frac{R_{C,CNT/probe} + R_{C,CNT/cat}}{n_{contact}}. \quad (2)$$

Plotting R_T against l_{CNT}, the normalized contact resistance $R_{C,total}$ corresponds to the R_T intercept. The determined contact resistance $R_{C,total}/n_{contact}$ was 6–15 kΩ, where the intercept of the black lines corresponds to the contact resistance.

To extract $R_{C,total}$, it is necessary to evaluate $n_{contact}$, which can be roughly expressed as

$$n_{contact} \approx S_{contact}/S_{CNT}, \quad (3)$$

where $S_{contact}$ and S_{CNT} are the CNT/nanoprobe contact area and area occupied by a hexagonally packed individual CNT, respectively. Here, the CNTs were assumed to be partially packed at the points of lowest resistance. $S_{contact}$ and S_{CNT} can be calculated as

$$S_{\text{contact}} = \pi d_{\text{contact}}^2/4, \text{ and} \quad (4)$$

$$S_{\text{CNT}} = \frac{\sqrt{3}}{2}(d_{\text{CNT}} + \delta)^2, \quad (5)$$

respectively, where d_{contact}, d_{CNT}, and δ correspond to the diameter of the contact area, CNT diameter, and interlayer distance of graphite ($\sim$0.34 nm), respectively. Because the curvature radius of the conductive probe is less than 25 nm, d_{contact} can be assumed to be 10–15 nm, as discussed later. Because d_{CNT} was 2.5 nm,[35] n_{contact} is evaluated to be 11–25. This range is consistent with the results determined from the measured CNT conduction above. Therefore, n_{contact} is $\sim$15, and $R_{\text{C,total}}$ is calculated to be 8×10^4–3×10^5 Ω.

The CNT bundle/nanoprobe contact resistivity should be normalized by the total contact length of the CNT wall edge $n_{\text{contact}}c_{\text{contact}}$.[23] The contact length of the individual CNT wall edge c_{contact} is roughly equal to

$$c_{\text{contact}} \approx \pi d_{\text{CNT}} n_{\text{wall}}. \quad (6)$$

Here, n_{wall} is the number of walls of the multi-walled CNTs. Because single-walled CNTs are dominant in our RPECVD CNT forest, c_{contact} corresponds to the circumference of an individual CNT. Because d_{CNT} is 2.5 nm, c_{contact} is evaluated to be $\sim$8 nm. The normalized individual CNT/metal contact resistivity $\rho_{\text{C,total}}$ can be expressed as

$$\rho_{\text{C,total}} = R_{\text{C,total}} c_{\text{contact}}. \quad (7)$$

Thus, $\rho_{\text{C,total}}$ was evaluated to be 6×10^5–2.4×10^6 Ω nm. In addition, the calculated contact resistivity for each end C atom[23] is 2.4×10^6–1×10^7 Ω·C atom. Note that this range includes the resistivities of both the top and bottom contacts of the CNTs; both the CNT/nanoprobe contact resistivity and CNT/catalyst contact resistivity should be lower than this range. It is not clear whether the top or bottom contact resistivity is the dominant component, but the contact resistivities of both ends are at most of the order of 10^7 Ω·C atom.

To verify this result, we compared it with the contact resistivity obtained from numerical studies. Some studies using first-principle quantum mechanics calculated that the CNT end/metal contact resistivity was $\sim 10^5$ Ω·C atom.[23,39,40] The difference of contact resistivity for each end C atom on the contacting metal is not as large as a factor of 2.5. The contact resistivity between the CNT ends and the C-AFM nanoprobe is 1–2 orders of magnitude higher than that determined from calculations. This is because theoretical studies have calculated the situation where dangling bonds of C atoms directly connect to a metal surface, whereas actual CNT ends have spacing molecules. A CNT end cut by CMP has dangling bond or be terminated like C-H, C-OH, and C-O-C. If the contact resistivity can be described as the tunneling resistance between the metal and CNT end, the tunneling resistance is drastically increased by spacing molecules.[22] Therefore, the contact resistivity may be decreased by cleaning the CNT edge or under a high contact pressure. Further investigation is necessary to determine the effects of CNT end termination and cleaning on contact resistance.

Determining the contact resistivity normalized by area is important for the electrical application of CNT wiring. We calculated the contact resistivity normalized by cross-sectional area. By multiplying by the cross-sectional area of CNTs, the calculated contact resistivity for a 2.5-nm-diameter single-walled CNT is 6×10^{-9}–2.1×10^{-8} Ω cm^2. Because this value depends on both the CNT diameter and wall number, it is important to increase the CNT density and wall number to decrease the contact resistivity.

A CNT sidewall contact has higher contact resistivity than a CNT end contact. The reported resistivity for a CNT cylindrical sidewall/metal film contact is 5×10^{-6} Ω cm^2 for a CNT/Ti-Au contact.[23] The end contact resistivity is 2–3 orders of magnitude lower than the experimental side contact resistivity, and this trend corresponds to that of the numerical studies.[24] The difference between the resistivities of CNT sidewall and end contacts originates from the distance between the metal and CNT electron clouds, because the conduction between contacting metals can be described as tunneling conduction. Tunneling resistivity increases exponentially as the tunneling distance increases. Matsuda and colleagues calculated that the atomic distance from the metal was 2.2–3.5 Å for a CNT sidewall contact[25] and 1.5–1.8 Å for a CNT end contact.[24] Tunneling occurs between the π electron cloud of a CNT sidewall and metal electron cloud for a CNT sidewall/metal contact and between the σ electron cloud of a C atom at the CNT end and metal electron cloud for a CNT end/metal contact. Here, the σ electron cloud at the CNT end acts as a mediator for electron tunneling between the CNT π electron cloud and metal electron cloud.[24] The actual electron tunneling distance is not clear, but the magnitude relationship of the tunneling distance should be similar to that of the atomic distance. Reported values for the contact resistivity between CNTs and metals are summarized in Table I.

We also investigated the contact properties of the VI structure by C-AFM. Figures 4(a) and 4(b) show SEM and C-AFM images of a CNT VI structure, respectively. VI structures with an 80-nm diameter and CNT length of 270 nm had a high resistivity of 67 kΩ. This CNT-VI structure exhibited a current of 0.12 μA under an applied voltage of 8 mV, as shown in Fig. 4(b). Here, because the width of the conductive region was 90–95 nm, the conductive region was wider than the actual VI diameter by 10–15 nm, as shown in Fig. 4(c). This is because the tip of the C-AFM nanoprobe had a large radius of curvature, so the conductive area was increased by the contact diameter.

The contact resistivity of multi-walled CNTs in a VI structure was evaluated. Because the CNT length in the VI structure was short compared to that of the RPECVD CNT forest, the ratio of the CNT resistance was small. Therefore, the contact resistance of the CNT via is assumed to be $\sim$67 kΩ. Here, the multi-walled CNTs in the VI structure did not form large bundles and existed independently in the SOG,[18] so the C-AFM nanoprobe should contact with the edge of about two multi-walled CNTs. If the CNT diameter and number of walls are 7 nm and seven,[18] respectively, the contact resistivity normalized by contacting CNT wall length is $\sim 2 \times 10^7$ Ω nm, which is one order of magnitude higher

TABLE I. Summary of reported CNT/metal contact resistivities.

Reference	E/T[a]	Contact type	CNT wall type	Contacting metal	Contact resistivity[b]		
					Per unit area (Ω cm^2)	Per end length (Ω nm)	Per C atom (Ω·C atom)
Lan[23]	E	Sidewall	Multi	Ti/Au	6×10^{-5}	…	…
					…	…	9×10^5 (Ti)
							9×10^6 (Pd)
		Sidewall					3×10^7 (Pt)
							6×10^8 (Cu)
							1×10^9 (Au)
Matsuda[24]	T		Single	Ti, Pd, Pt, Cu, Au	…	$(4 \times 10^5$ (Ti))	1×10^5 (Ti)
						$(6 \times 10^5$ (Pd))	1×10^5 (Pd)
		End				$(6 \times 10^5$ (Pt))	1×10^5 (Pt)
						$(1 \times 10^6$ (Cu))	3×10^5 (Cu)
						$(7 \times 10^5$ (Au))	2×10^5 (Au)
Gao[39]	T	End	Single	Cu	1.5×10^{-11}	…	(4×10^5)
Chiodarelli[27]	E	End	Multi	Ti/Au	(8×10^{-7})	…	…
Yokoyama[18]	E	End	Multi	Ti/Cu	$3–8 \times 10^{-8}$		
Inaba[22]	E	Sidewall	Multi	CNT	10^{-8}	…	…
Inaba[33]	E	End	Multi	n-SiC[c]	$\sim 10^{-4}$	…	…
This work	E	End	Single	$PtIr_5$	$6 \times 10^{-9}–2.1 \times 10^{-8}$	$6 \times 10^5–2.4 \times 10^6$	$2.4 \times 10^6–1 \times 10^7$

[a]E: Experimental study, T: Theoretical study.
[b]Numbers in parentheses were evaluated from the results reported in the papers.
[c]n-SiC is a semiconductor.

than that determined for the single-walled RPECVD CNT forest.

We also considered the end contact system in which a metal top electrode was deposited on the VI structure. Yokoyama *et al.*[18] reported the resistivity normalized by the area of VI structures. Because the lowest resistivity of an interconnect with micrometer-order diameter and CNT density were 3–8 Ω μm^2 and 1.6×10^{11} cm^{-2}, respectively, the resistance of individual multi-walled CNTs was 0.5–1.3 $\times 10^4$ Ω. As mentioned above, the top/bottom contact resistances are large. The calculated contact resistivity normalized by contacting CNT wall length is 0.8–2 $\times 10^6$ Ω nm, which corresponds to that determined for the RPECVD CNT bundle. Therefore, the top electrode can form a better contact with the CNT ends than the C-AFM probe for multi-walled CNTs.

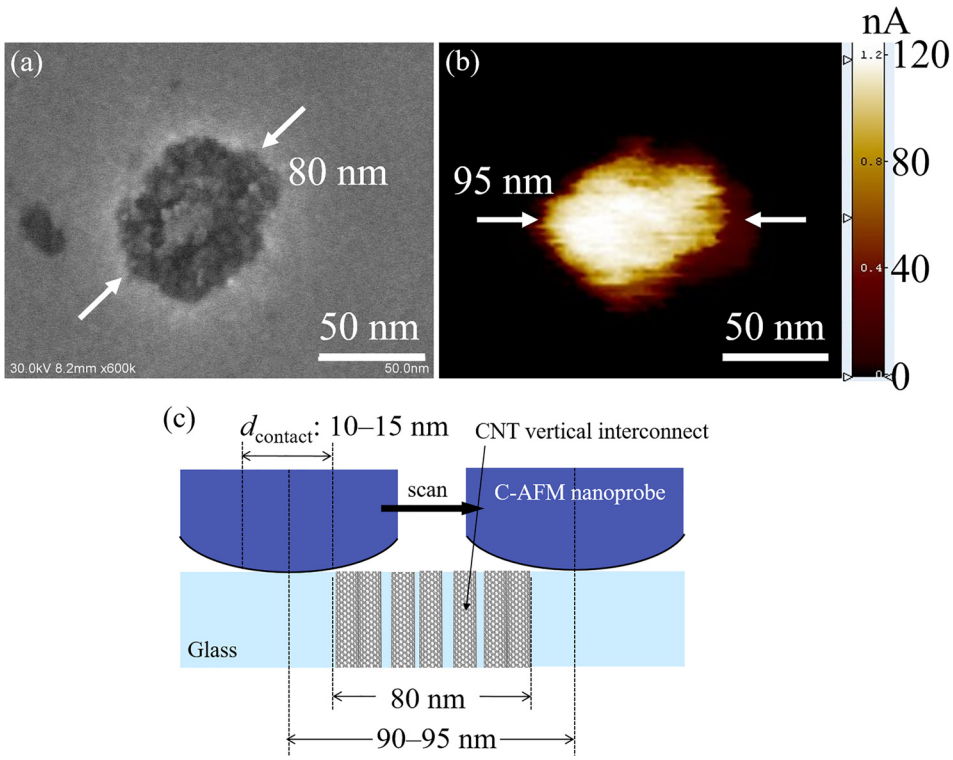

FIG. 4. (a) SEM image of an 80-nm-diameter VI structure. (b) C-AFM image of the equivalent VI structure. (c) Schematic of the contact formed between the C-AFM nanoprobe and CNT VI structure. The width of the current conduction area was 90–95 nm. Thus, the estimated diameter of the CNT/nanoprobe contact area was 10–15 nm.

We wished to determine why the C-AFM probe had high contact resistivity with the multi-walled CNTs. When the C-AFM nanoprobe contacted single-walled CNTs, the contact resistivity was similar to the case of top electrode contacts for multi-walled CNTs. Single-walled CNTs were distorted by the pressure from the C-AFM probe when the CNT end (not sidewall) contacted the C-AFM nanoprobe. Because the RPECVD CNT forest was mainly single-walled CNTs, the CNTs and their bundles were highly flexible and their ends could fit to the shape of the C-AFM nanoprobe, which improved the contact between them. In contrast, individual multi-walled CNTs were rigid and the C-AFM nanoprobe could not properly contact with all the inner walls. If the C-AFM nanoprobe only contacts with the outermost wall of a multi-walled CNT, which means that n_{wall} in Eq. (6) is 1, the contact resistivity normalized by the contacting CNT wall is calculated to be $\sim 3 \times 10^6\ \Omega$ nm, which is of the same order of magnitude as that for a single-walled CNT bundle. Although the detailed contact properties for multi-walled CNT ends were not clear, the C-AFM nanoprobe has the potential to form effective contacts with CNT ends if the CNTs are flexible enough to fit the shape of the contacting nanoprobe tip.

CONCLUSION

We experimentally investigated the contact resistivity between CNT ends and a metal nanoprobe by C-AFM. A homogenous electrical contact was formed for a CNT forest on SiC/C-AFM probe system. In contrast, current maps of the RPECVD CNT forests were not homogeneous and had high-current peaks starting from zero current. The transfer length method was applied to a processed RPECVD CNT forest to measure the CNT/metal contact resistance. Assuming that some CNTs contacted the C-AFM nanoprobe, the contact resistivity normalized by the CNT end contact length was found to be $0.6\text{–}2.4 \times 10^6\ \Omega$ nm, which is 1–2 orders of magnitude higher than the result of a theoretical study. The contact resistivity of the CNT end contact normalized by contact area was 2–3 orders of magnitude lower than that reported for CNT sidewall contact. For a multi-walled CNT VI structure, the measured contact resistivity was one order of magnitude higher than that of a RPCVD CNT forest, but the contact resistivity of the top metal electrode was similar to that of the RPECVD CNT forest. Our results showed that C-AFM nanoprobes have the ability to form contacts with CNT ends if the CNTs are flexible enough to fit the shape of the contacting nanoprobe tip.

SUPPLEMENTARY MATERIAL

See supplementary material for the topographic image of vertical interconnect structure and the planar view of CNT forest after chemical mechanical polishing.

ACKNOWLEDGMENTS

This study was supported by the Japan Society for the Promotion of Science KAKENHI (Grant No. 26630136) and Research Fellowship for Young Scientists (17J08746). We thank Natasha Lundin, Ph.D., from the Edanz Group (www.edanzediting.com/ac) for editing a draft of this manuscript.

[1]P. Avouris, Chem. Phys. **281**, 429 (2002).
[2]Z. Yao, C. L. Kane, and C. Dekker, Phys. Rev. Lett. **84**, 2941 (2000).
[3]Y. Awano, S. Sato, D. Kondo, M. Ohfuti, A. Kawabata, M. Nihei, and N. Yokoyama, Phys. Status Solidi A **203**, 3611 (2006).
[4]D. Yokoyama, T. Iwasaki, T. Yoshida, H. Kawarada, S. Sato, T. Hyakushima, M. Nihei, and Y. Awano, Appl. Phys. Lett. **91**, 263101 (2007).
[5]N. Chiodarelli, Y. Li, D. J. Cott, S. Mertens, N. Peys, M. Heyns, S. De Gendt, G. Groeseneken, and P. M. Vereecken, Microelectron. Eng. **88**, 837 (2011).
[6]J. C. Coiffic, D. Mariolle, N. Chevalier, S. Olivier, D. Lafond, M. Fayolle, S. Maitrejean, and H. Le Poche, Appl. Phys. Lett. **92**, 223510 (2008).
[7]C. Subramaniam, T. Yamada, K. Kobashi, A. Sekiguchi, D. N. Futaba, M. Yumura, and K. Hata, Nat. Commun. **4**, 2202 (2013).
[8]M. Nihei, M. Horibe, A. Kawabata, and Y. Awano, Jpn. J. Appl. Phys., Part 1 **43**, 1856 (2004).
[9]S. Sato, M. Nihei, A. Mimura, A. Kawabata, D. Kondo, H. Shioya, T. Iwai, M. Mishima, M. Ohfuti, and Y. Awano, in *Interconnect Technology Conference* (2006), p. 230.
[10]T. Wang, K. Jeppson, L. Ye, and J. Liu, Small **7**, 2313 (2011).
[11]M. Katagiri, Y. Yamazaki, M. Wada, M. Kitamura, N. Sakuma, M. Suzuki, S. Sato, M. Nihei, A. Kajita, and T. Sakai, Jpn. J. Appl. Phys., Part 1 **50**, 05EF01 (2011).
[12]A. Okamoto, I. Gunjishima, T. Inoue, M. Akoshima, H. Miyagawa, T. Nakano, T. Baba, M. Tanemura, and G. Oomi, Carbon **49**, 294 (2011).
[13]Y. Yamazaki, M. Katagiri, N. Sakuma, M. Suzuki, S. Sato, M. Nihei, M. Wada, N. Matsunaga, T. Sakai, and Y. Awano, Appl. Phys. Express **3**, 055002 (2010).
[14]G. Zhong, J. H. Warner, M. Fouquet, A. W. Robertson, B. Chen, and J. Robertson, ACS Nano **6**, 2893 (2012).
[15]N. Na, D. Kim, Y. So, Y. Ikuhara, and S. Noda, Carbon **81**, 773 (2015).
[16]A. Srivastava, X. Liu, and Y. Banadaki, *Carbon Nanotubes for Interconnects* (Springer, 2017), pp. 37–80.
[17]J. Li, Q. Ye, A. Cassell, H. Ng, R. Stevens, J. Han, and M. Meyyappan, Appl. Phys. Lett. **82**, 2491 (2003).
[18]D. Yokoyama, T. Iwasaki, K. Ishimaru, S. Sato, T. Hyakushima, M. Nihei, Y. Awano, and H. Kawarada, Jpn. J. Appl. Phys., Part 1 **47**, 1985 (2008).
[19]M. Katagiri, M. Wada, B. Ito, Y. Yamazaki, M. Suzuki, M. Kitamura, T. Saito, A. Isobayashi, A. Sakata, and N. Sakuma, Jpn. J. Appl. Phys., Part 1 **51**, 05ED02 (2012).
[20]C. Li, E. T. Thostenson, and T. Chou, Appl. Phys. Lett. **91**, 223114 (2007).
[21]S. Gong, Z. H. Zhu, and E. I. Haddad, J. Appl. Phys. **114**, 074303 (2013).
[22]M. Inaba, C. Lee, K. Suzuki, M. Shibuya, M. Myodo, Y. Hirano, W. Norimatsu, M. Kusunoki, and H. Kawarada, J. Phys. Chem. C **120**, 6232 (2016).
[23]C. Lan, P. Srisungsitthisunti, P. B. Amama, T. S. Fisher, X. Xu, and R. G. Reifenberger, Nanotechnology **19**, 125703 (2008).
[24]Y. Matsuda, W. Deng, and W. A. Goddard III, J. Phys. Chem. C **114**, 17845 (2010).
[25]Y. Matsuda, W. Deng, and W. A. Goddard III, J. Phys. Chem. C **111**, 11113 (2007).
[26]J. Li, R. Stevens, L. Delzeit, H. Ng, A. Cassell, J. Han, and M. Meyyappan, Appl. Phys. Lett. **81**, 910 (2002).
[27]N. Chiodarelli, M. Sugiura, Y. Kashiwagi, Y. Li, K. Arstila, O. Richard, D. J. Cott, M. Heyns, S. D. Gendt, G. Groeseneken, and P. M. Vereecken, Nanotechnology **22**, 085302 (2011).
[28]A. Schulze, T. Hantschel, A. Dathe, P. Eyben, X. Ke, and W. Vandervorst, Nanotechnology **23**, 305707 (2012).
[29]W. Wu, S. Krishnan, T. Yamada, X. Sun, P. Wilhite, R. Wu, K. Li, and C. Y. Yang, Appl. Phys. Lett. **94**, 163113 (2009).
[30]K. Li, R. Wu, P. Wilhite, V. Khera, S. Krishnan, X. Sun, and C. Y. Yang, Appl. Phys. Lett. **97**, 253109 (2010).
[31]M. Kusunoki, M. Rokkaku, and T. Suzuki, Appl. Phys. Lett. **71**, 2620 (1997).
[32]G. Zhong, T. Iwasaki, K. Honda, Y. Furukawa, I. Ohdomari, and H. Kawarada, Jpn. J. Appl. Phys., Part 1 **44**, 1558 (2005).

[33]M. Inaba, K. Suzuki, M. Shibuya, C. Lee, Y. Masuda, N. Tomatsu, W. Norimatsu, A. Hiraiwa, M. Kusunoki, and H. Kawarada, Appl. Phys. Lett. **106**, 123501 (2015).
[34]G. Zhong, T. Iwasaki, and H. Kawarada, Carbon **44**, 2009 (2006).
[35]M. Myodo, M. Inaba, K. Ohara, R. Kato, M. Kobayashi, Y. Hirano, K. Suzuki, and H. Kawarada, Appl. Phys. Lett. **106**, 213503 (2015).
[36]T. Iwasaki, J. Robertson, and H. Kawarada, Nano Lett. **8**, 886 (2008).
[37]S. V. Kalinin and A. Gruverman, *Scanning Probe Microscopy* (Springer, New York, 2007), pp. 82–85.
[38]M. R. Maschmann, Carbon **86**, 26 (2015).
[39]F. Gao, J. Qu, and M. Yao, Appl. Phys. Lett. **96**, 102108 (2010).
[40]F. Gao, J. Qu, and M. Yao, J. Electron. Packag. **133**, 020908 (2011).